RESEARCH PAPERS

Acta Cryst. (1995). B51, 149–155

Electron-Microscope Study of the Structure of Ag_8S Formed in the Initial Stage of Silver Sulfidation

BY Y. D. YU AND R. GUAN

Laboratory of Atomic Imaging of Solids, Institute of Metal Research, Academia Sinica, Shenyang 110015, *People's Republic of China*

AND H. HASHIMOTO AND Y. MAKITA

Faculty of Engineering, Okayama University of Science, Okayama 700, *Japan*

(*Received* 19 *June* 1994; *accepted* 1 *August* 1994)

Abstract

The atomic positions in the unit cell of metastable silver sulfide, Ag_8S, formed in the initial stage of sulfidation of silver, have been studied by high-resolution electron microscope images and selected-area electron diffraction patterns, interpreted by electron diffraction and image formation theories. The unit cell belongs to the orthorhombic system with space group *Imm*2. The lattice parameters are $a = 0.59$, $b = 0.64$ and $c = 0.87$ nm.

1. Introduction

It is well known that some metals form a series of metastable suboxides with oxygen contents much lower than the usual oxides in the initial stage of oxidation. For instance, many different copper oxides such as Cu_4O (Guan, Hashimoto & Yoshida, 1984), Cu_8O (Guan, Hashimoto & Kuo, 1984) and $Cu_{64}O$ (Guan, Hashimoto & Kuo, 1985) have been proposed. Similar results have also been obtained in the initial stage of oxidation of the nickel crystal (Ishii & Hashimoto, 1967), where the compositions Ni_8O (Guan, Lu, Kuo & Hashimoto, 1986) and $Ni_{64}O$ (Guan, Hashimoto & Kuo, 1989) have been determined. Since such suboxides are in general only a few microns in size, their structures can hardly be analyzed by the normal X-ray diffraction methods. Conventional high-resolution electron transmission microscopes enable us to obtain the structural information of such oxides by combining the selected-area electron diffraction methods. In particular, when the crystal contains both heavy and light atoms, the dynamical scattering of electron waves can reveal only the position of the light atoms in some thicknesses of the specimen, and hence the crystal structure analysis can be carried out effectively (Guan, Hashimoto & Kuo, 1986).

In chemical terms, the oxidation of metals means a change in the valence state of the metal atoms or ions, which become more positively charged. In this broader sense, the reaction of metals with sulfur or a halide is the same as the metal oxidation process. Therefore, metal sulfidation, like oxidation, is a basic problem in metal corrosion. For silver, sulfidation is more important than oxidation in material engineering processes, such as in microelectronics. The corrosion of silver in the atmosphere is decisively influenced by the type and content of pollutants in the air. Among air contaminants, SO_2, H_2S *etc.* are commonly regarded as the most harmful (Abbott, 1974). Although these reactive gases are present in sub-p.p.m. levels in an ordinary environment, sulfidation is the major cause of silver corrosion in polluted atmospheres (Franey, Kammlott & Graedel, 1985). In a laboratory investigation of the tarnishing of silver in the presence of H_2S, SO_2 *etc.*, the rate of sulfidation has been investigated in detail (Shiojiri, Maeda & Murata, 1969; Volpe & Peterson, 1989). However, according to our knowledge, no similar works concerning the structure of silver sulfide in the initial sulfidation stage have been reported so far.

In the present paper, we report the formation of the sub-sulfide phase Ag_8S prior to the formation of Ag_2S.

2. Experimental procedures and observation

A block of pure silver (purity 99.99 wt.%) was cold-rolled into sheets of *ca* 50 μm in thickness and then electrolytically thinned by the window method in a solution of 20% nitric acid and 80% absolute alcohol. The thin foil specimen was then placed in a sealed tube, where a trace of sulfur was left on the tube wall. This tube was then evacuated to *ca* 10^{-2} Pa. When the temperature of the furnace

reached 573 K, the sealed tube was quickly introduced into it, and at the same time, the power supply was cut off. Details of the experimental procedure are similar to Rickert's method (1959). After being cooled to room temperature, these thin films were examined in a JEM-200CX electron microscope equipped with a top-entry goniometer stage and a pole piece ($C_s = 1.2$ mm) having a point-to-point resolution of 0.25 nm. Many microcrystallites of sulfide formed at the edge of the film. Figs. 1(*a*) and (*b*) are low-magnification electron microscope images of these sulfide crystallites. The arrows in Fig. 1(*a*) show some minute crystallites growing out of the edge of a crystallite. Fig. 1(*b*) shows sulfide crystals grown in the cavity, which was not in the matrix before sulfidation. Fig. 1(*c*) shows similar crystallites which were obtained by heating a silver film in air on a large pure silver plate by an alcohol lamp. It was also noted that when the silver films were stored in air, for example for more than 3 months, similar crystallites were formed even without heating, as shown in Fig. 1(*d*). By comparing the selected-area electron diffraction patterns (SAED) of these films with those of silver and known silver sulfides, it becomes clear that these crystallites are neither the crystallites of pure silver nor the known silver sulfides. Thus, they may belong to a new silver sulfide. Fig. 1(*e*) shows the characteristic X-ray peaks obtained from the crystallites in Fig. 1(*c*) using an energy-dispersive X-ray spectrometer (EDXS), and indicates that the crystallites contain sulfur of about 2–3 wt.%, which is much lower than the sulfur content of 12.9 wt.% in Ag_2S. Thus, for convenience, these crystallites are referred to as Ag_xS ($x > 2$).

In the present work, the specimens prepared using the three methods described above were investigated similarly.

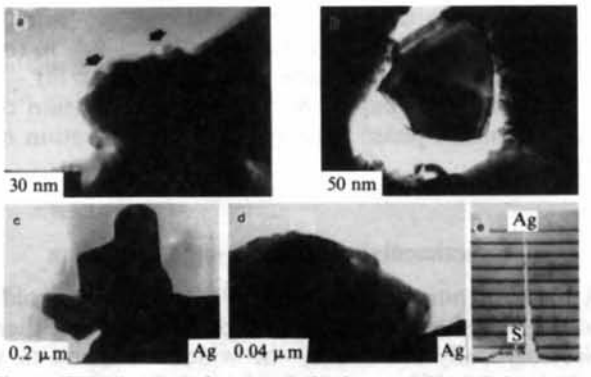

Fig. 1. TEM images of: (*a*) and (*b*) the crystal Ag_xS formed by heating at 537 K in a vacuum of 10^{-2} Pa with a trace of sulfur; (*c*) the crystal formed by slightly heating the silver film in air; (*d*) a thin crystal of Ag_xS formed at room temperature in air for *ca* 3 months; (*e*) X-ray spectrum from the crystal shown in (*c*), showing the peaks of sulfur and silver.

3. Crystallographic consideration

Figs. 2(*a*)–(*f*) show a series of SAED patterns from the sulfidized silver specimens in different orientations, among which Fig. 2(*a*) was observed more frequently. Fig. 3 is made artificially by the superposition of the two SAED patterns of Ag_xS in Fig. 2(*a*) and silver in a [110] orientation. The strong spots are from the silver lattice. It is obvious that the lattice spacings of Ag_xS are approximately twice as large as that of silver. This phenomenon is similar to the case of Cu_8O and Cu (Guan, Hashimoto & Kuo, 1984). Based on the analyses for Cu_8O and also on the SAED patterns in Fig. 3, a two-dimensional structure model of Ag_8S is presented in Fig. 4(*a*), as the projection of silver along [110]. By checking the extinction of the diffraction spots in Figs. 2(*a*)–(*f*), it was noted that the S atoms form the body-centered orthorhombic unit cell with $a = 0.59$, $b = 0.64$ and $c = 0.87$ nm.

Table 1 shows the ratio of two basic reciprocal-lattice vectors $\mathbf{g}_1$ ($h_1k_1l_1$) and $\mathbf{g}_2$ ($h_2k_2l_2$). The corre-

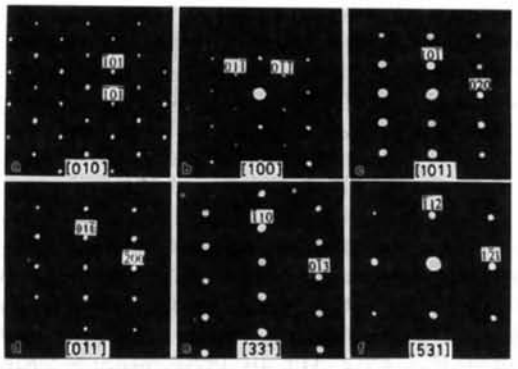

Fig. 2. SAED patterns of Ag_xS for six different orientations. Indices are based on the orthorhombic unit cell shown in Figs. 4(*a*) and (*b*).

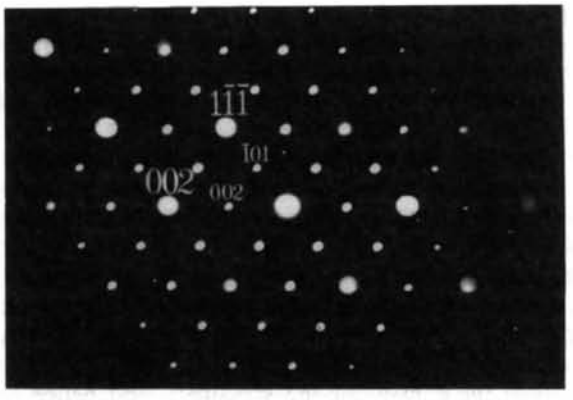

Fig. 3. The artificial superposition of the two SAED patterns of Ag_8S [010] (weak spots) and silver [110] (strong spots). The strong spots indexed by the large letters belong to silver.

Table 1. *Analysis of the electron diffraction patterns with reference to the* Ag_8S *crystal structure*

[uvw]	$(h_1k_1l_1)$	$(h_2k_2l_2)$	$g_2(h_2k_2l_2)/g_1(h_1k_1l_1)$ Calculated	Observed	φ (°) Calculated	Observed
010	$\bar{1}01$	$\bar{1}0\bar{1}$	1.00	1.00	68.3	68.5
100	$01\bar{1}$	$0\bar{1}\bar{1}$	1.00	1.00	107.3	107.2
101	$10\bar{1}$	020	1.54	1.57	90.0	90.5
011	$01\bar{1}$	$\bar{2}00$	1.74	1.68	90.0	90.6
331	$\bar{1}10$	$0\bar{1}3$	1.64	1.68	106.3	105.9
531	$\bar{1}12$	$1\bar{2}1$	1.15	1.12	114.9	115.0

Table 2. *Atomic coordinates of* Ag *and* S *in the unit cell (space group Imm*2)

Element	Multiplicity	Wyckoff letter	Coordinates of equivalent positions $(0, 0, 0; \frac{1}{2}, \frac{1}{2}, \frac{1}{2})+$	x, y, z
Ag(1)	4	(d_1)	$0, y, z; 0, \bar{y}, z$	$y=\frac{1}{4}, z=\frac{1}{8}$
Ag(2)	4	(d_2)	$0, y, z; 0, \bar{y}, z$	$y=\frac{3}{4}, z=\frac{1}{8}$
Ag(3)	4	(c_1)	$x, 0, z; \bar{x}, 0, z$	$x=\frac{1}{4}, z=\frac{3}{8}$
Ag(4)	4	(c_2)	$x, 0, z; \bar{x}, 0, z$	$x=\frac{3}{4}, z=\frac{1}{8}$
S	2	(a)	$0, 0, z$	$z=0$

sponding direction of the incident beam is shown as [*uvw*] in Table 1. The angles which have been obtained from the proposed model and from the SAED patterns are also shown in Table 1, indicating good agreement. The relationship between the unit cell of Ag_xS and that of silver is shown in Fig. 4(*a*) as the projection of (110) silver. The origin of the coordinates is placed at the S atoms, in order to clearly show the characteristics of the body-centered orthorhombic structure. The unit-cell perspective of Ag_xS is shown in Fig. 4(*b*), together with the unit cells of silver to gain a better understanding of the relationship between these two crystals. The small black discs and large circles represent the Ag and S atoms, respectively. The atomic position is shown in Table 2, which satisfies the space group *Imm*2.

In this structure, S atoms locate in the center of the tetrahedra consisting of four Ag atoms. The ratio of the number of Ag to S atoms in this structure is 8:1, and thus Ag_xS should be depicted as Ag_8S.

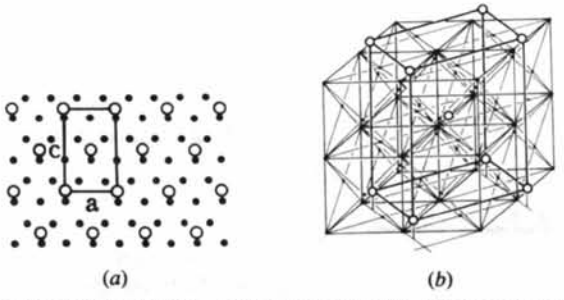

(*a*) (*b*)

Fig. 4. (*a*) [010] projection of the structure of Ag_8S. The unit cell is outlined by thick lines. (*b*) A perspective of the orientation relationship between the unit cell of Ag_8S (thick lines) and that of silver (thin lines). The orthorhombic unit cell depicted by thick lines is the unit cell of Ag_8S. The black small discs and large circles represent the Ag and S atoms, respectively.

4. Comparison of the observed and calculated data

The proposed model of Ag_8S should be confirmed by a comparison of the observed images and the diffraction patterns with the simulated ones, calculated on the basis of the dynamical theory of electron diffraction and image formation theory.

Since Ag_8S has uniform thickness and the same orientation is limited to an area of only a few nanometers, observed intensities of the selected area of diffraction patterns (*ca* 100 nm^2 area) become the averaged values and the image intensities become different in each local area, as shown in Fig. 5. The regions marked by *A* and *B* in Fig. 5 have different thicknesses, which is seen by the background darkness, *i.e.* dark region *A* is thicker than bright region *B*. Moreover, region *B* shows some local intensity change, which seems to be due to the small thickness and/or orientation change. In order to compare the intensity distribution of observed local images with the calculated images, the value of the local specimen thickness must be known together with the electron optical condition of image recording, which can be measured experimentally.

Although the techniques used to observe the cross-section of the specimen and the spacing of the subsidiary maxima of convergent-beam diffraction patterns can give the specimen thickness in specific ranges of thickness and area, the application of these techniques is very difficult in the present case because of the small size, Bragg reflection condition and surface roughness of the local sulfide crystal grains. Thus, in the present observation, a number of systematic simulated image calculations have been carried out over the thickness ranges 0.64 (one unit cell) to 30.7 nm (48 unit cells), with one unit cell difference and defocus values of 40.0, 55.0 (Scherzer focus), 78.0, 98.0 and 110.0 nm. The total calculated images were 288 frames. By comparing the calculated images and observed images of specimen areas *A* and

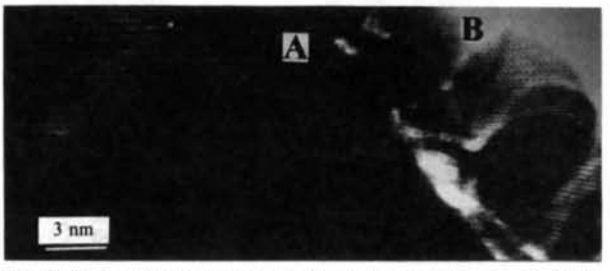

Fig. 5. [010] HREM images of Ag_8S showing the crystal lattice structures with a different image contrast in the different areas. Region *A* is seen to be thicker than region *B*.

B in Fig. 5, it was noted that images of good fit have thicknesses between 28.2 (44 unit cells) and 29.4 nm (46 unit cells) for region *A* in Fig. 5, and between 0.64 (one unit cell) and 1.92 nm (3 unit cells) for region *B* in Fig. 5, as shown in Figs. 6 and 7, respectively. One of the calculated images was then chosen from Figs. 6 and 7, respectively, and arranged in Figs. 8(*c*) and (*d*), together with magnifications of regions *A* and *B* in Fig. 5 as (*a*) and (*b*). The contrast of the calculated and observed images is in good agreement. The electron optical condition used for the image simulation was as follows: chromatic defocus value $\Delta = 17.0$ nm, semi-angle of convergence of the incident beam $\alpha_c/\lambda = 0.3$ rad nm^{-1}, and the size of the objective aperture $\sin\theta/\lambda = 1/2d = 3.50$ nm^{-1}. Δf 98.0 and 66.0 nm for these images, respectively. From these defocus values (underfocus) and specimen thicknesses, the imaging configuration becomes as shown in Fig. 9.

Good agreement of simulated images and observed images can be understood by considering the thickness dependence of amplitudes and phases of several fundamental diffracted waves.

Fig. 10(*a*) shows the variation between the amplitudes of several diffraction waves from the Ag_8S crystal in the [010] orientation *versus* thickness. The amplitudes of the waves from (202) and (004), which mainly consist of Ag atoms, become larger with increasing thickness, oscillate for a period of *ca* 4.5 nm, but the waves from (200), (101), (002) and (103), which have half-spacing atomic planes between their planes with different reflecting power, increase almost monotonically with increasing thickness. With a thickness of 1.3 nm, the amplitudes of the diffracted waves from (202) and (004) are larger than those from (200), (101), (002) and (103), as seen in Fig. 10(*a*). Since the amplitudes of the waves from (202) and (004) are strong and the phases of all the waves are almost equal, as seen in Fig. 10(*b*), the intensity distribution for the bottom face of the specimen crystal becomes rather strong for the Ag-atom position and weak for the S-atom position. However, these positions are not clearly resolved because of the small separation of the Ag and S

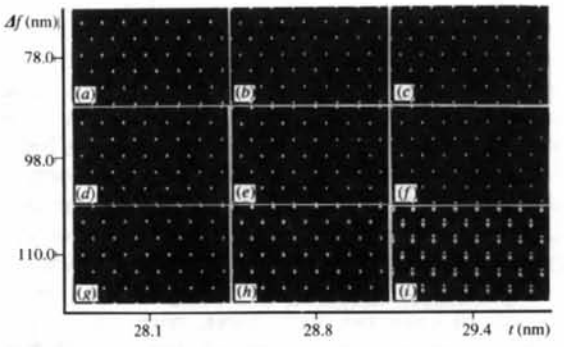

Fig. 6. Calculated image contrasts for $\Delta f = 78.0$, 98.0 and 110.0 nm and thicknesses $t = 28.1$, 28.8 and 29.4 nm.

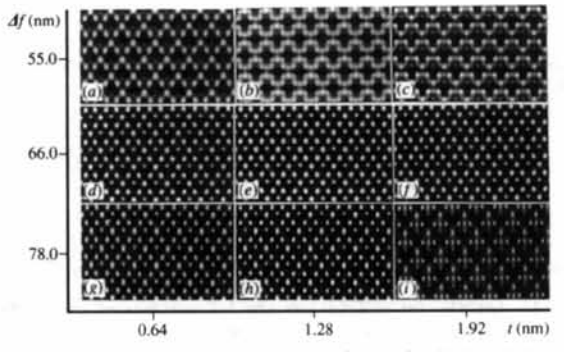

Fig. 7. Calculated image contrasts for $\Delta f = 55.0$, 66.0 and 78.0 nm and thicknesses $t = 0.64$, 1.28 and 1.92 nm.

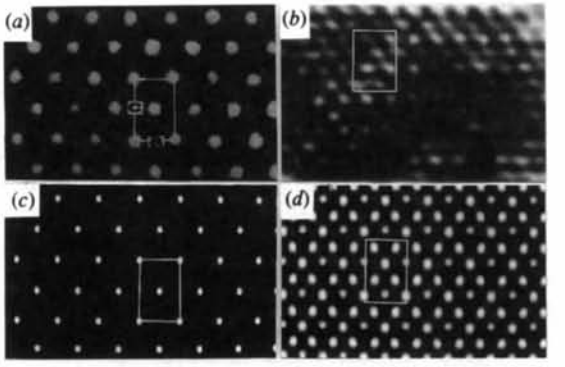

Fig. 8. Comparison of the observed and calculated images of Ag_8S. (*a*) and (*b*) are the magnified images, taken from the areas *A* and *B* in Fig. 5, respectively. (*c*) and (*d*) are the calculated images, with the thickness 28.8 nm, defocus $\Delta f = 98.0$ nm and 1.28 nm, $\Delta f = 66.0$ nm. Calculation condition, see text.

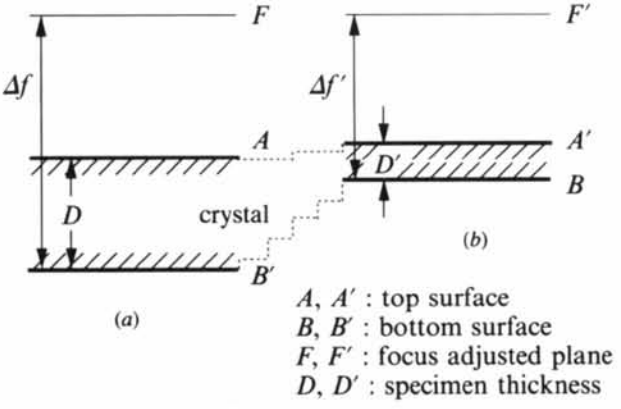

Fig. 9. Schematic illustration of imaging configuration: (*a*) and (*b*) correspond to the regions *A* and *B* in Fig. 5. $\Delta f = 98.0$ nm, $D = 29.0$ nm, $\Delta f' = 66.0$ nm, $D' = 1.3$ nm.

atoms, thus the bright spots correspond to the Ag-atom positions, but they appear at a shifted position, as shown in Figs. 8(*b*) and (*d*). At the thickness 29.0 nm, the amplitudes from most of the waves except (004) have appreciably large values and contribute to the image intensity by interfering with each other. At this thickness, as seen in Fig. 10(*b*), phases of the waves from (202), which mainly consist of Ag atoms, are almost zero and other waves which consist of both S and Ag atoms have almost the same π values, *i.e.* ($\lambda/2$). Thus, by the interference of these waves, the subtraction of the information regarding Ag-atom position, which are in (202) reflections, from the information on S- and Ag-atom position, which are in (200), (101), (002) and (103) reflections, occurs and only the S-atom position is projected on the bottom face of the crystal.

Although the diffraction patterns from the small selected area (*e.g.* 10 nm) are rather difficult to obtain, it is easy to make Fourier transform (FT) patterns of the observed and simulated images. This can be used for checking the intensity of the diffracted waves, contributing to the electron microscope images. Figs. 11(*a*), (*b*), (*c*) and (*d*) are the FT patterns from observed and simulated images of Ag_8S, as shown in Figs. 8(*a*), (*b*), (*c*) and (*d*), respectively. Figs. 11(*e*) and (*f*) are schematic illustrations of (*a*), (*c*) and (*b*), (*d*), respectively. By comparing these patterns, it is seen that the intensities of the diffracted waves, which have contributed to the image intensity, are almost equal, respectively. In Fig. 11(*b*), the spots from $(\bar{2}02)$ and $(20\bar{2})$ are weak, which are due to the small specimen area in the symmetry position, as can be seen in Fig. 8(*b*). It can also be seen clearly that the spots from (004) and (202) are stronger, which are expected from Fig. 10(*a*), and with a large surrounding area in the asymmetry position. The electron microscope images are produced by the interference of diffracted waves, including (000) waves. Since the waves which are scattered with equal angles to the optical axis have high coherency, their contribution to the image intensity becomes high. The degree of coherence between the diffracted waves was taken into account in the calculation as the transmission cross coefficients (TCC) of the two individual waves (Ishizuka, 1982). Thus, the FT patterns of both the recorded images and calculated images are not the same as the electron diffraction patterns, as shown in Fig. 2,

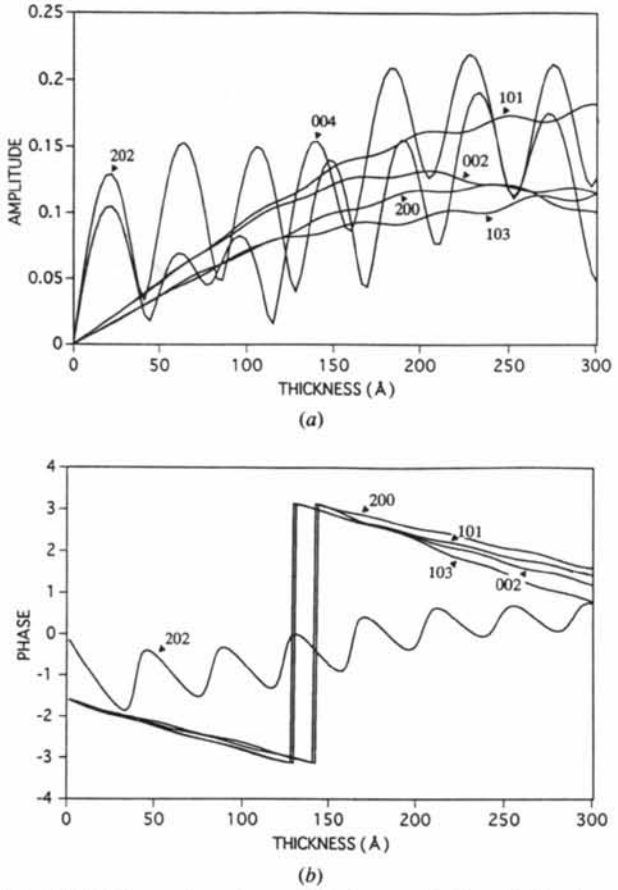

Fig. 10. Thickness dependence of (*a*) the amplitudes and (*b*) phase of the diffracted waves from (101), (002), (200), (103), (202) and (004) of the Ag_8S crystal in the [010] orientation. For details, see text.

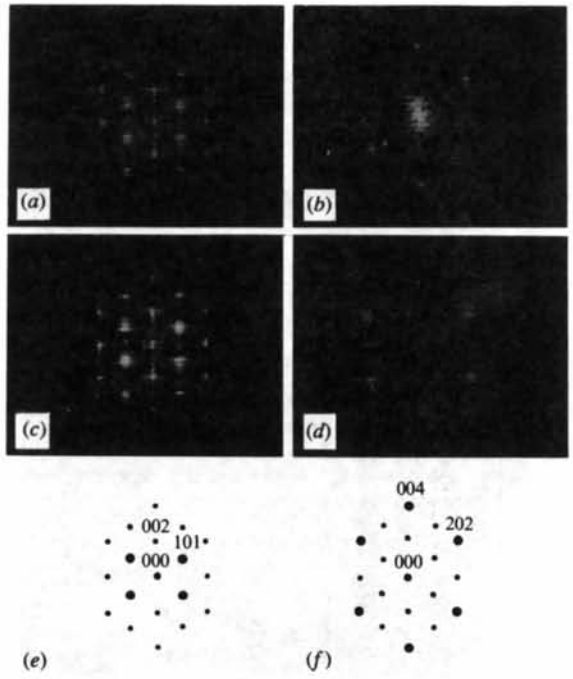

Fig. 11. (*a*), (*b*), (*c*) and (*d*) are the FT patterns of the electron microscope images shown in Figs. 8(*a*), (*b*), (*c*) and (*d*), respectively. (*e*) and (*f*) are the schematic illustrations of (*a*), (*c*) and (*b*), (*d*), respectively.

which is the intensity (square of amplitude) of individual diffraction waves. Since the FT patterns of the electron microscope image are expressed as

$$Ig = \sum_{g} Tg_1g_2Qg_1Q^*g_2, \quad (1)$$

where Tg_1g_2, Qg_1 and Qg_2 are TCC, amplitudes of diffracted waves $\mathbf{g}_1$ and $\mathbf{g}_2$, respectively, and * represents the complex conjugate; FT of the images and the diffraction patterns have close correlation.

A high-resolution image projected along the [101] direction of this crystal is shown in Fig. 12. The electron diffraction pattern of this orientation is shown in Fig. 2(*c*). The two-dimensional projection of the crystal structure along this direction is also shown, in which small black discs represent Ag atoms and large open circles represent S atoms. The simulated image of Ag_8S along this direction is also shown in Fig. 8 as an insert. The parameters used in this calculation are: defocus $\Delta f = 95$ nm and specimen thickness $t = 13.6$ nm. The other parameters are as in the previous [010] image simulation.

Agreement between the observed and calculated images in the [010] and [101] orientations and the FT patterns in the [010] orientation is rather good, which suggests that the proposed structural model of Ag_8S is correct.

5. Discussion

The present investigation confirms the formation of Ag_8S crystals in the initial stage of the sulfidation of silver. Although the S-atom positions in the crystal have not yet been directly confirmed by using an image-filtering atom resolution electron microscope, which utilizes the electron energy loss spectrum, it can be concluded from the contrast of the images, the intensity distribution of FT patterns and X-ray spectroscopy that the reaction is sulfidation rather than oxidation even in the case of heating in air.

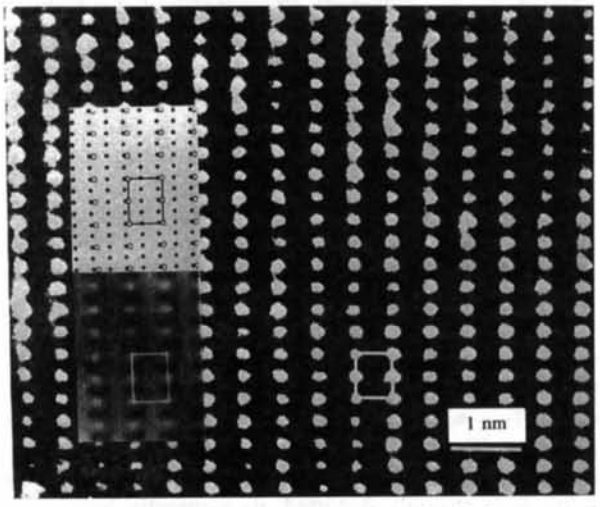

Fig. 12. [101] magnified HREM image of Ag_8S with inserts of the simulated image and the structure model, which corresponds well with the observed image. For calculation condition, see text.

The sulfidation, like oxidation, is a diffusion-controlled process involving the inward movement of anions. The formation of Ag_8S, analogous to Cu_8O, may occur by a process in which S atoms enter into silver interstice. Since the noble metals have generally high defect formation energy, it is difficult to form a large volume of Ag_8S crystals and only very little sulfur can react with silver. When the content of sulfur is increased, the crystal becomes unstable under critical conditions such as electron irradiation, as was observed in the case of Ag_2S. Thus, it can be concluded that Ag_8S can exist as stable crystals and can be formed by the reaction of silver with a trace of sulfur compound gases in air, such as SO_2 and H_2S *etc.*

The selected electron diffraction patterns obtained in the present observation are from *ca* 100 nm^2 in area. The thicknesses of the Ag_8S crystals formed are different, even if they are single crystals, as can be seen in Fig. 5, and the intensities of the diffracted waves are highly dependent on thickness. Thus, the diffraction patterns shown in Fig. 2 have an averaged intensity from the crystal of *ca* 100 nm. As can be seen from Figs. 8(*a*) and (*b*), if a crystal thickness ranges from 1.0 to 30.0 nm, which is seen actually in Fig. 5, the integrated intensities of each diffracted wave from this crystal region with different thicknesses become almost equal, as can be seen in Fig. 2(*a*), and not proportional to the scattering powers of the planes concerned. However, the FT patterns shown in Figs. 11(*a*) and (*b*) are seen to be equivalent to the diffraction patterns of the observed crystal region with a certain thickness. However, it must be noted here that the electron microscope images are formed by interference between diffracted waves and the contribution to the image intensity is highly dependent on the degree of coherence between the two waves concerned, as shown in (1). By understanding the difference and similarity, the FT patterns can be used as the replacement for electron diffraction patterns. Due to the above considerations, in the present observation, a comparison of FT patterns was made rather than comparing the observed and calculated diffraction patterns.

The tetrahedral interstice space in the silver lattice has a diameter of only 0.118 nm. When a neutral S atom with the radius 0.102 nm or a S ion with the radius 0.185 nm enters the tetrahedral interstice space, expansion of the lattice will be produced. In the present observation, the unit cell of Ag_8S expands 2, 11 and 6% in the *a*, *b* and *c* axes, respectively, in terms of matrix silver lattice.

The authors would like to express their thanks to Professors K. H. Kuo and H. Endoh for their encouragement and comments. The present work is partly supported by National Natural Science Foundation of China. One of the authors (YDY) would like to express sincere thanks to Inoue Foundation for Science, for the support to work by staying in Japan.

References

ABBOTT, W. H. (1974). *IEEE Trans. Parts Hybrids Packag.* **10**, 24–27.
FRANEY, J. P., KAMMLOTT, G. W. & GRAEDEL, T. E. (1985). *Corros. Sci.* **25**, 133–143.
GUAN, R., HASHIMOTO, H. & KUO, K. H. (1984). *Acta Cryst.* B**40**, 560–566.
GUAN, R., HASHIMOTO, H. & KUO, K. H. (1985). *Acta Cryst.* B**41**, 219–225.
GUAN, R., HASHIMOTO, H. & KUO, K. H. (1986). *Ultramicroscopy*, **20**, 195–202.
GUAN, R., HASHIMOTO, H. & KUO, K. H. (1989). *Solid State Phenom.* **5**, 73–84.
GUAN, R., HASHIMOTO, H. & YOSHIDA, T. (1984). *Acta Cryst.* B**40**, 109–114.
GUAN, R., LU, J., KUO, K. H. & HASHIMOTO, H. (1986). Proc. XIth Int. Congr. on Electron Microscopy, Kyoto, Japan, pp. 831–832.
ISHII, M. & HASHIMOTO, H. (1967). *Jpn. J. Appl. Phys.* **6**, 173–180.
ISHIZUKA, K. (1982). *Acta Cryst.* A**38**, 773–779.
RICKERT, H. (1959). *Z. Phys. Chem.* **21**, 432–435.
SHIOJIRI, M., MAEDA, S. & MURATA, Y. (1969). *Jpn. J. Appl. Phys.* **8**, 24–31.
VOLPE, L. & PETERSON, P. J. (1989). *Corros. Sci.* **29**, 1179–1196.

Acta Cryst. (1995). B**51**, 155–161

The Crystal and Molecular Structure of Dodecahydridosilasesquioxane, $H_{12}Si_{12}O_{18}$

BY KARL WILHELM TÖRNROOS

Structural Chemistry, Stockholm University, 106 91 *Stockholm, Sweden*

HANS-BEAT BÜRGI

Institut für Chemische und Mineralogische Kristallographie, Universität Bern, 3012 *Bern, Switzerland*

AND GION CALZAFERRI AND HERIBERT BÜRGY

Institut für Anorganische, Analytische und Physikalische Chemie, Universität Bern, 3000 *Bern* 9, *Switzerland*

(*Received* 23 *February* 1994; *accepted* 22 *November* 1994)

Abstract

The title compound belongs to a family of cage-shaped spherosiloxane molecules which show, as a common and systematic feature, smaller or larger distortions from their respective ideal point-group symmetry. By means of statistical methods in combination with rigid-body analysis, the molecular distortions involved in the lowering of the molecular symmetry of $H_{12}Si_{12}O_{18}$ and $(C_6H_5)_{12}Si_{12}O_{18}$ have been analysed. The magnitudes and types of the deformations may be described in terms of a small number of symmetry displacement coordinates involving displacement of flexibly joined, but otherwise rigid, corner-sharing tetrahedra.

Introduction

In a series of studies the geometries of spherosilasesquioxane molecules are being analysed. Previous papers have reported results for $H_8Si_8O_{12}$ (Auf der Heyde, Bürgi, Bürgy & Törnroos, 1991; Törnroos, 1994; Törnroos, Schwarzenbach, Larsen & Delley, 1995), $Cl_8Si_8O_{12}$ (Törnroos, Calzaferri & Imhof, 1995), $H_{10}Si_{10}O_{15}$ (Bürgi, Törnroos, Calzaferri & Bürgy, 1993), $Co(CO)_4H_7Si_8O_{12}$ (Calzaferri, Imhof & Törnroos, 1993) and $(C_6H_{13})H_7Si_8O_{12}$ (Calzaferri, Imhof & Törnroos, 1994). The structures of two isomers, D_{3h} ($\bar{6}m2$) and C_{2v} (mm), of $H_{14}Si_{14}O_{21}$ have been previously reported by Agaskar, Day & Klemperer (1987). This report describes $H_{12}Si_{12}O_{18}$, pictured in Fig. 1. The molecular connectivity shows four ten-membered rings and four eight-membered rings of alternating Si and O atoms. In zeolite language, where only the Si atoms are counted, it would be four five- and four four-membered rings, see scheme (*a*) below. The highest attainable point-group symmetry of this molecule is D_{2d} ($\bar{4}2m$). In the crystalline state the molecule is strongly distorted, its symmetry being only C_1 (1). A second type of arrangement of this structure is also possible, namely that of two six-rings bridged by six O atoms, with molecular symmetry D_{6h} ($6/mmm$), see